An Analytical Model of Water Diffusion and Exchange in White Matter from Diffusion MRI and Its Application in Measuring Axon Radii

Wenjin Zhou, *Student Member, IEEE*, and David H. Laidlaw, *Senior Member, IEEE*

Abstract— We present an analytical model of water diffusion and exchange in white matter for estimating axon radii. Estimates of direct microstructural features such as axon radii, density, and permeability are important for early disease detection. Our model for white matter has two compartments between which there is an exchange of water molecules. Our analytical formulas examine the derivation of microstructure parameters that affect signal attenuation in diffusion-weighted MR experiments in white matter. The model is fitted to six constant-gradient diffusion-MRI experiments based on Monte-Carlo simulation with gradient strength $200-700$ (mT/m). Our results demonstrate the feasibility of recovering underlying axon radii of $[1, 1.9, 3, 5, 7]$ (μm) using the model. Axon radii are typically in the range $[0.25-10]$ (μm) in brain tissue. Our work is aimed at non-invasively recovering microstructure features using a geometric model that incorporates water exchange.

Index Terms—diffusion MRI; axon radii, microstructure, restricted diffusion, neural tissue, white matter

1 Introduction

Diffusion MRI measures the displacement of water molecules within tissue over a fixed time interval. We can derive information about the tissue microstructure from measurements of the water molecules' displacement over time. Common biomarkers derived from diffusion MRI, such as mean diffusivity (MD) and fractional anisotropy (FA), are useful indicators of major microstructural changes, but they are non-specific at the microstructural level: changes in FA can result from changes in axon density, radius distribution, orientation, or permeability, and we cannot distinguish among these possibilities. Furthermore, different combinations of changes in these microstructure features may result in no change in FA at all. Axon radii directly affect different nerve functions. In myelinated axons, nerve conduction velocity is directly proportional to axon radii [12] [14]. Therefore, estimates of direct microstructural features such as axon radii could provide insights into brain diseases and aid in their early detection.

This paper develops a new composite analytical model for water diffusion and exchange in white matter from diffusion MRI and a procedure to recover the microstructure model parameters, mainly axon radii, using Markov chain Monte Carlo (MCMC). We discuss some previous approaches in recovering axon radii in the next section. Section 3 outlines our analytical model of water diffusion and exchange from diffusion MRI and its derivation. The simulation data and results in sections 4 and 5 assess the feasibility and accuracy with which we estimate axon radii and other direct microstructure features from the model. We discuss our findings and draw conclusions in sections 6 and 7.

2 Related Work

Despite their importance, axon radii have not been reliably measurable in vivo. Electron microscopy is currently considered the most accurate way to obtain axon radii distribution. However, it is an invasive histological procedure and can access only a limited area of a tissue section. Tissue preparation is difficult and tedious and the results are subject to many artifacts, including tissue shrinkage and cracking.

One approach to measuring axon radii uses diffraction patterns from the diffusion-MRI signal in vivo. This approach has been controversial, however: while diffraction patterns have recovered correct radii in some cases [3], in others they do not reflect the mean axon radius as measured microscopically [15]. L*ä*tt et al. [8] concluded that 10 (μm) is the smallest identifiable radius using diffusion patterns with current hardware. This suggests a difficulty in measuring axon radii using diffraction patterns, since they are typically in the range $0.25-10$ (μm) in brain tissue [1].

A recent alternative approach formulates a geometric model of white-matter microstructures and predicts the MR signal from water diffusing within the model. The model typically has two compartments: intra- and extra-axonal volumes. Model-based techniques potentially demonstrate microstructural features such as axon radii and their distribution, diffusion coefficients of the water molecules, etc., and can thus estimate distinct microstructure features simultaneously. Previous work [1] [2] showed that diffusion MRI can provide estimates of features such as axon radii. However, to simplify the model, all previous techniques assumed no exchange of water between the intra- and extra-axonal compartments. This constraint on water exchange could restrict accurate extraction of radii distribution of very small ($\approx 2\mu m$) and very large ($\approx 20\mu m$) axons. In addition, experimental results have indicated that exchange of water molecules between compartments does occur [13][7][10]. Recent work [9] has also demonstrated that if diffusion is modeled by two compartments of which one is restricted, exchange must be included in the model.

Here we develop a new geometric model of water in white matter that integrates diffusion and exchange of water molecules between axonal compartments. Our results, based on Monte-Carlo simulation data, demonstrate the feasibility of recovering underlying axon radii using the model. Our work is a first attempt at non-invasively recovering microstructure features incorporating water exchange.

3 Model for Water Diffusion in White Matter

Our model for white matter has two compartments between which there is an exchange of water molecules. The model assumes parallel non-abutting cylindrical axon cells with equal radii and partially permeable membranes embedded in an extra-cellular medium. MR signal attenuation reflects water diffusion in white matter by two processes: restricted water diffusion within the cylindrical intra-axonal space and hindered water diffusion outside the cylinders, in the extra-axonal space (Fig. 1). We use subscript and superscript 1 and 2 to denote the intra-axonal and extra-axonal compartments, respectively.

• *Wenjin Zhou and David H. Laidlaw are with the Department of Computer Science at Brown University, E-mail:{wzhou, dhl}@cs.brown.edu.*

The normalized MRI signal is then

$$E(\vec{q},\Delta) = \upsilon E_1(\vec{q},\Delta) + (1-\upsilon)E_2(\vec{q},\Delta) \quad (1)$$

where

- $E(\vec{q},\Delta)$ is the total observed diffusion signal decay
  - wavenumber $\vec{q} = \gamma\delta\vec{G}$, γ is the gyromagnetic ratio, δ is the pulse duration, and $\vec{G}$ is the applied gradient
  - Δ is the diffusion time between pulses in MRI experiments
- E_1 and E_2 represent the signal decay of water molecules in the intra- and extra-axonal compartments, respectively
- $\upsilon \in [0,1]$ is the volume fraction of the intra-axonal compartments

Sections 3.1 and 3.2 below demonstrate how we derive the signal decay of water molecules in the intra- and extra-axonal compartments (E_1 and E_2 respectively). Section 3.3 summarizes our composite model.

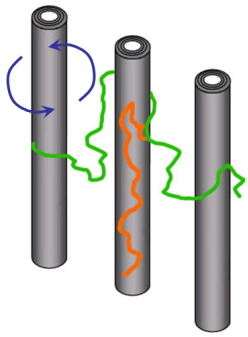

Fig. 1. Modeling of water diffusion in white matter by two processes: restricted water diffusion within the cylindrical intra-axonal space and hindered water diffusion outside the cylinders in the extra-axonal space.

3.1 Water Diffusion in the Intra-axonal Space

In order to determine how water diffusion affects signal attenuation in diffusion-weighted MR experiments in white matter, we examine the conditional propagator and the conditions in the intra-axonal space that govern the motion of the water molecules.

Propagators for water diffusion

The motion of molecules undergoing diffusion can be described by the conditional propagator, $P_s(\vec{r}_0|\vec{r},t)$, an ensemble-averaged probability density for spin displacement from $\vec{r}_0$ to $\vec{r}$ over time t. $P_s(\vec{r}_0|\vec{r},t)$ obeys:

- The Fick's Law differential equation governing $P_s(\vec{r}_0|\vec{r},t)$:

$$\frac{\partial P_s^{(1)}}{\partial t} = D_1 \nabla^2 P_s^{(1)} \quad (2)$$

- The initial condition $P_s(\vec{r}_0|\vec{r},t)$ for spin displacement from $\vec{r}_0$ to $\vec{r}$ over time t:

$$P_s^{(1)}(\vec{r}_0|\vec{r},0) = \delta(\vec{r}-\vec{r}_0) \quad (3)$$

- Boundary condition for partially permeable membranes:

$$D_1 \frac{\partial P_s^{(1)}}{\partial \rho}|_{\rho=a} + M P_s^{(1)}|_{\rho=a} = 0 \quad (4)$$

- Boundary relationship of the intra- and extra-cellular compartments:

$$D_1 \frac{\partial P_s^{(1)}}{\partial \rho}|_{\rho=a} = D_2 \frac{\partial P_s^{(2)}}{\partial \rho}|_{\rho=a} \quad (5)$$

where D_1 and D_2 are free diffusion coefficients and a is axon radius.

Boundary condition for partially permeable membranes (Eq. (7))
The boundary condition describes the displacement probability at the membrane. In the partially permeable membrane condition [4], we may confine our consideration to the molecules that do not leave the cylinder [11]. Once they have left, their contribution to the echo signal with increasing field gradient intensities drops to zero as a function of q. Thus, we derive the corresponding boundary condition Eq. (7), where $M(m/s)$ is the permeability coefficient. Below we shall see that it is convenient to relate the microscopic reduced permeability h of an axon of radius a to the permeability coefficient as:

$$h = \frac{aM}{D_1} \quad (6)$$

Boundary relationship of the intra and extra-cellular compartments (Eq. (5))
The boundary relationship describes the diffusion flux density at two sides of the membrane. The diffusion equation must satisfy both the above boundary condition and boundary relationship. The Fick's Law diffusion equation (2) can be rewritten as:

$$\frac{\partial P_s}{\partial t} = \nabla \cdot (D \cdot \nabla P_s) \quad (7)$$

If we define diffusion flux density as:

$$\vec{j} = -D \cdot \nabla P_s \quad (8)$$

Eq. (7) is then:

$$\frac{\partial P_s}{\partial t} + \nabla \cdot \vec{j} = 0 \quad (9)$$

Eq. (9) is equivalent to the continuity equation in electrodynamics, which implies that the normal component of $\vec{j}$ on the boundary should be continuous:

$$\vec{n} \cdot (\vec{j}_1 - \vec{j}_2) = j_{1n} - j_{2n} = 0 \quad (10)$$

$\vec{j}_1$ and $\vec{j}_2$ indicate $\vec{j}$ on two sides of the boundary, respectively.

We denote the normal component of $\vec{j}$, j_n. By definition of $\vec{j}$,

$$j_n = -D \frac{\partial P_s}{\partial n}|_s \quad (11)$$

In the cylindrical coordinate system, the outward surface normal $\vec{n}$ direction is in the direction along the polar axis direction (i.e. across a diameter). Therefore, we derive our boundary relationship Eq. (5) from Eqs. (10) and (11):

$$D_1 \frac{\partial P_s^{(1)}}{\partial \rho}|_{\rho=a} = D_2 \frac{\partial P_s^{(2)}}{\partial \rho}|_{\rho=a}$$

MRI signal attenuation in the intra-axonal compartment

The diffusion problem posed in Eqs. (2)-(5) above may be solved using the standard eigenmode expansion [5]:

$$P_s^{(1)}(\vec{r}_0|\vec{r},t)) = \sum_{n=0}^{\infty} C_n e^{-\lambda_n t} u_n(\vec{r}_0) u_n^*(\vec{r}) \quad (12)$$

where the $u_n(\vec{r})$ are orthonormal sets of solutions to the Helmholtz equation parameterized by the eigenvalue λ_n. Based on our Cauchy

boundary condition in Eq. (7), which specifies a linear combination of the values that a solution of a differential equation can take on the boundary of the domain and the normal derivative at the boundary, the problem is well posed. Given the input and the cylindrical boundary limits to the problem, there exists a unique discrete eigenvalue solution.

We solve the problem in a cylindrical coordinate system in which the longitudinal z axis is a symmetry axis for the system. The relevant coordinates are (ρ, φ) and the gradient is applied along the polar axis direction (i.e. across a diameter). Eq. (12) becomes:

$$P_s^{(1)}(\vec{r}_0|\vec{r},t) = \sum_{n=0}^{\infty} C_n e^{-\lambda_n t} J_n(k_\rho \rho_0) J_n(k_\rho \rho) e^{in(\varphi-\varphi_0)} \tag{13}$$

The permeable membrane boundary is at a radial distance $r = a$ from the cylinder center. For notational convenience, we define the roots k_ρ of the Bessel function J_n as $k_\rho = \frac{\alpha_{nm}}{a}$. Considering our boundary condition Eq. (7), the eigenfunction expansion for the propagator is then given by:

$$\begin{aligned} P_s^{(1)}(\vec{r}_0|\vec{r},t) = \sum_{n=0}^{\infty}\sum_{m=1}^{\infty} A_{nm}^2 e^{\frac{-\alpha_{nm}^2 D_1 \Delta}{a^2}} J_n(\frac{\alpha_{nm}}{a}\rho_0) J_n(\frac{\alpha_{nm}}{a}\rho) \\ \times \cos(n\varphi_0)\cos(n\varphi) \end{aligned} \tag{14}$$

where J_n are the standard (cylindrical) Bessel functions, while the eigenvalues α_{nm} are determined by the boundary condition Eq. (7), which is:

$$\frac{\alpha_{nm} J_n'(\alpha_{nm})}{J_n(\alpha_{nm})} = -h \tag{15}$$

A_{nm} are normalizing constants:

$$A_{0m}^2 = \frac{1}{\pi a^2} \frac{\alpha_{0m}^2}{J_0^2(\alpha_{0m})(h^2+\alpha_{0m}^2)} \tag{16}$$

$$A_{nm}^2 = \frac{2}{\pi a^2} \frac{\alpha_{nm}^2}{J_n^2(\alpha_{nm})(h^2+\alpha_{nm}^2-n^2)}, n \neq 0 \tag{17}$$

The derivation of Eq. (15)-(17) is developed in detail in Appendices A and B.

Finally, we can derive the echo attenuation in Q-space by applying Fourier transformation on the propagator function in X-space Eq. (14):

$$\begin{aligned} E_1(\vec{q},\Delta) &= \int\int \rho(r,0) P_s^{(1)}(\vec{r}_0|\vec{r},\Delta) e^{i2\pi\vec{q}\cdot(\vec{r}-(\vec{r}_0))} d\vec{r}_0 d\vec{r} \\ &= \sum_{m=1}^{\infty} 4e^{\frac{-\alpha_{0m}^2 D_1 \Delta}{a^2}} \frac{\alpha_{0m}^2}{h^2+\alpha_{0m}^2} \frac{[2\pi qa J_0'(2\pi qa) + hJ_0(2\pi qa)]^2}{[(2\pi qa)^2 - \alpha_{0m}^2]^2} \\ &\quad + \sum_{n=1}^{\infty}\sum_{m=1}^{\infty} 8e^{\frac{-\alpha_{nm}^2 D_1 \Delta}{a^2}} \frac{\alpha_{nm}^2}{h^2+\alpha_{nm}^2-n^2} \\ &\quad \times \frac{[2\pi qa J_n'(2\pi qa) + hJ_n(2\pi qa)]^2}{[(2\pi qa)^2 - \alpha_{nm}^2]^2} \end{aligned} \tag{18}$$

In a typical experiment, only the lowest eigenvalue $\alpha = \alpha_{01}$ is important [11]. Thus, for the purpose of measuring the axon radii, we can simplify the echo attenuation equation, (18), and Eq. (15) becomes:

$$\frac{\alpha_{01} J_0'(\alpha_{01})}{J_0(\alpha_{01})} = -h \tag{19}$$

According to the Bessel function, $J_n'(x) = (\frac{n}{x})J_n(x) - J_{n+1}(x)$, we can derive $J_0'(x) = -J_1(x)$. Therefore, our final derivation of the boundary condition is:

$$\frac{\alpha_{01} J_1(\alpha_{01})}{J_0(\alpha_{01})} = h \tag{20}$$

We can approximate $\frac{\alpha_{01}^2}{h^2+\alpha_{01}^2} = 1$ similarly. Our final simplified MRI signal attenuation in the intra-axonal compartment is:

$$E_1(\vec{q},\Delta) = 4e^{\frac{-\alpha_{01}^2 D_1 \Delta}{a^2}} \frac{[hJ_0(2\pi qa) - 2\pi qa J_1(2\pi qa)]^2}{[(2\pi qa)^2 - \alpha_{01}^2]^2} \tag{21}$$

where a is axon radius and all other parameters have the meanings above.

3.2 Water Diffusion in the Extra-axonal Space

By applying a Fourier transformation on the Fick's Law differential equation (2) governing $P_s(\vec{r}_0|\vec{r},t)$ in X-space, we can derive differential equations describing echo signal intensities in Q-space:

$$\frac{\partial E(\vec{q},t)}{\partial t} = -q^2 D E(\vec{q},t) \tag{22}$$

The solution to the equation has the form $E(\vec{q},t) = E_0 e^{-q^2 Dt}$. Therefore, we model the hindered diffusion surrounding the axons with Gaussian distribution. By assuming a large exchange time τ, $q^2\tau D_2 \gg 1$, the apparent diffusion coefficient of the extra-axonal compartment can be approximated as $D_{2app} = D_2 + \frac{1}{q^2\tau}$ [8]. The MRI signal attenuation in the extra-axonal compartment is then:

$$E_2(\vec{q},\Delta) = e^{-q^2 D_2 \Delta + \frac{\Delta}{\tau}} \tag{23}$$

3.3 Composite Model for Water Diffusion in Axonal Space

In summary, referring to Eqs. (1), (21), and (23), our composite model for normalized MRI signals from water diffusion in axonal space is:

$$\begin{aligned} E(\vec{q},\Delta) &= \upsilon E_1(\vec{q},\Delta) + (1-\upsilon)E_2(\vec{q},\Delta) \\ &= \upsilon(4e^{\frac{-\alpha_{01}^2 D_1 \Delta}{a^2}} \frac{[hJ_0(2\pi qa) - 2\pi qa J_1(2\pi qa)]^2}{[(2\pi qa)^2 - \alpha_{01}^2]^2}) \\ &\quad + (1-\upsilon)(e^{-q^2 D_2 \Delta + \frac{\Delta}{\tau}}) \end{aligned} \tag{24}$$

with boundary condition

$$\frac{\alpha_{01} J_1(\alpha_{01})}{J_0(\alpha_{01})} = h \tag{25}$$

where

- J_n are the standard (cylindrical) Bessel functions and the eigenvalues α_{nm} are determined by boundary condition Eq. (15)

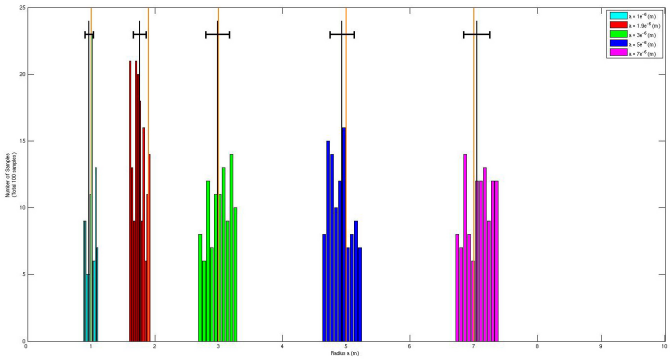

Fig. 2. Histogram of 100 samples drawn from posterior distribution on radii $a = [1, 1.9, 3, 5, 7]$ (μm) using MCMC; orange lines indicate the true value of various radii; black lines indicate the mean value of each estimate with error bars showing standard deviation. The model was fitted to six constant-gradient diffusion-MRI experiments based on Monte-Carlo simulation with gradient strength $200 - 700$ (mT/m). The results demonstrate the feasibility of recovering underlying axon radii using the model.

- experimental parameters are:
  - The wavenumber $\vec{q} = \gamma\delta\vec{G}$, γ is the gyromagnetic ratio, δ is the pulse duration, and $\vec{G}$ is the applied gradient
  - The time between pulses in MRI experiments is Δ
- The microstructure parameters are:
  - The axon radius, a
  - The volume fraction of the intra-axonal compartment $f \in [0,1]$
  - The free diffusion coefficients of the intra- and extra-axonal compartments respectively, D_1 and D_2
  - The permeability $h = \frac{Ma}{D}$ in the intra-axonal compartment; M is the permeability coefficient
  - The exchange time in the extra-axonal compartments, τ

4 Simulation Data

In order to estimate the underlying microstructure parameters and validate our model, we performed several experiments using simulation data. The benefit of using simulation data is that the ground truth about the microstructure parameters is known and controllable.

Our diffusion MRI simulation data was derived from Monte Carlo simulation of the geometric model with rectangular arrangement of cylinders using CAMINO [6]. Our model was fitted to six constant-gradient experiments with the following microstructure parameters: various cylindrical radii: $a = [1, 1.9, 3, 5, 7]$ (μm); the exchange rate $\tau = 0.6$ (s); the free diffusion coefficients of the intra-axonal and extra-axonal water were assumed to be the same, $D = 2e^{-9}$ (m^2/s); and the intra-axonal volume fraction $f = 0.708$. We set our experimental parameters to be: $\delta = 2$ (ms); diffusion time was chosen from 20 to 1060 (ms) with 14 linear increments; diffusion gradients were applied only perpendicular to the axon axis (i.e. across a diameter) and each simulation was repeated for six linear gradient amplitudes of $200 - 700$ (mT/m) with SNR = 16.

5 Results

We used a Markov chain Monte Carlo procedure to get samples of the posterior distribution of the model parameters given the data. We used broad uniform priors for all the scalar model parameters. Our proposed distributions were Gaussian with standard deviations chosen manually to give suitable acceptance rates. We initialized parameters to the true value to speed up convergence. The MCMC was run for 10,000 iterations, which yields approximately 100 independent samples from the marginal posterior distribution of model parameters.

Figures 2 and 3 show our main results. Each histogram combines a total number of 100 samples from MCMC runs. Figure 2 shows the histogram of the marginal posterior distribution on radii a for each of the various true $a = [1, 1.9, 3, 5, 7]$ (μm). As mentioned earlier, previous work [1] had much lower accuracy in recovery of smaller radii ($\approx 2\mu m$) compared to larger radii. Our study was able to recover radii at about the same variance for both small and large radii ($a = 1e^{-7} - 7e^{-7}$ (μm)). Figure 3 shows the histogram of the marginal posterior distribution of the other microstructure parameters f (volume fraction), D (free diffusion coefficient) and τ (exchange rate). In previous work [1], there was a downward bias in estimating the free diffusion coefficient D. We were able to recover the diffusion coefficient quite close to the true value. For comparison, the orange lines in the graph indicate the true value of the corresponding parameters from simulation data. The black vertical lines indicate the mean value of each estimation and their error bar corresponds to standard deviation. Overall, the estimate of the microstructure parameters is accurate and demonstrates the feasibility of recovering underlying microstructure radii.

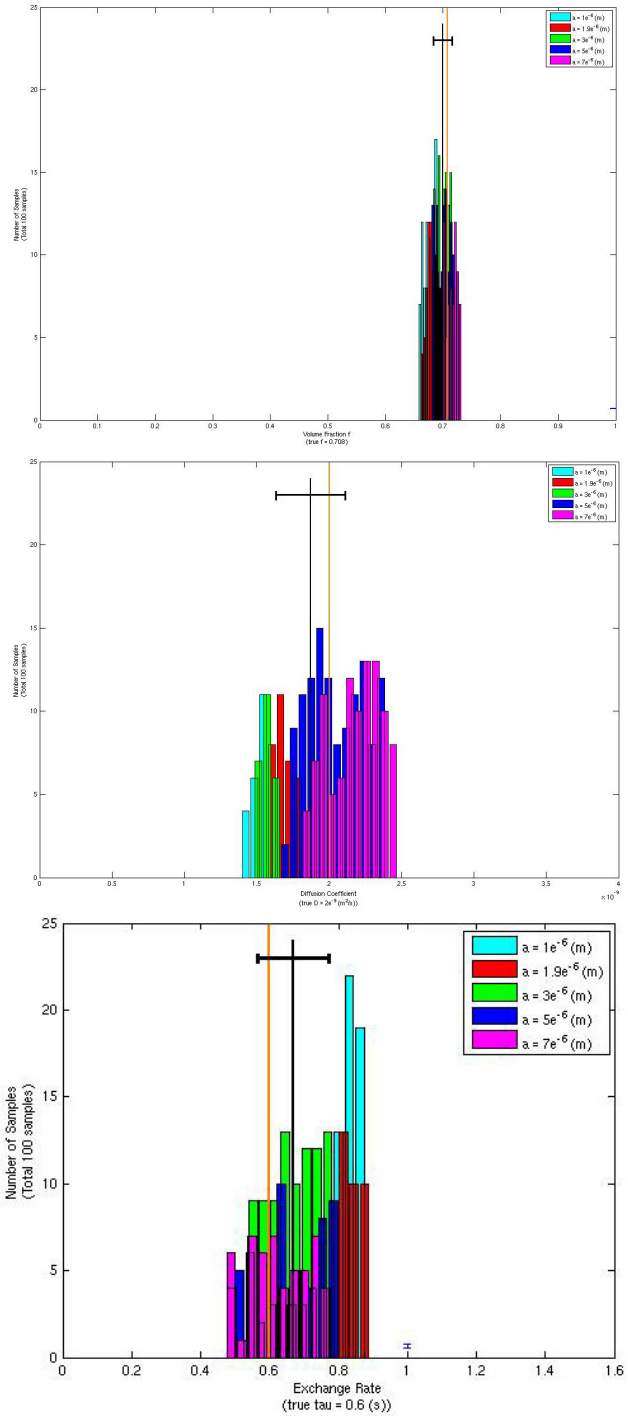

Fig. 3. Histogram of 100 samples drawn from posterior distributions on volume fraction f, free diffusion coefficient D, and exchange rate τ at various radii: $a = [1, 1.9, 3, 5, 7]$ (μm) with color coding as in Figure 2. The orange lines indicate the true value of $f = 0.708$, $D = 2e^{-9}$ (m^2/s) and $\tau = 0.6$ (s). The black lines indicate the mean value of each estimate with error bars showing standard deviation. Note that overlapping bars may not show on the figure.

6 Discussion

We show here that we can recover axon radii and other microstructural features such as volume fraction and diffusion coefficient using our model through a MCMC procedure. This lets us measure anatomical and microstructural features of tissue noninvasively with a more realistic model that integrates water exchange. Direct measurement

of axon radii could have a significant impact on our understanding of white matter architecture and connectivity and improve detection of abnormal development and changes.

Our model is based on two assumptions: (1) water diffusion within axon is restricted, and (2) water molecules exhibit a slow exchange rate. The first assumption, while not proven, is supported by much experimental evidence. It is reasonable to model the intra-axonal compartment of axons as a pack of cylinders containing water. The second condition is also supported by studies that show the exchange rate may be as high as $700ms$ [7].

Currently, a single value for the axon radius has been assumed per voxel for simplicity. This can easily be extended in the future to integrate over a model distribution of axon radii. Also, in the current model, we are assuming single axon direction per voxel. It could be extended to model the distribution for direction using spherical harmonic decomposition to detect fiber crossing and fiber kissing.

Our feasibility study of estimating direct microstructure features such as radii based on simulation data provides compelling results, but clearly requires further study. The next step is to apply our model to real macaque data. Our method will be validated with radii distributions measured from photomicrographs on the corpus callosum and the cingulum bundle.

7 Conclusion

We presented a new composite analytical model of diffusion and exchange of water in white matter from diffusion MRI. Our work is a first attempt to estimate microstructure features through diffusion MRI model incorporating water exchage. Our results demonstrate the feasibility of recovering underlying axon radii and other microstructure features such as volume fraction and diffusion coefficient using the model through the MCMC procedure from Monte Carlo simulation data. We were able to achieve higher accuracy in recovering small axon radii ($\approx 2\ \mu m$) and diffusion coefficient than in previous work.

APPENDIX A

This derivation shows how we formulate the boundary condition, Eq. (15). Based on our general solution to $P_s^{(1)}(\vec{r}_0|\vec{r},t)$ in Eq. (13):

$$P_s^{(1)}(\vec{r}_0|\vec{r},t) = \sum_{n=0}^{\infty} C_n e^{-\lambda_n t} J_n(k_\rho \rho_0) J_n(k_\rho \rho) e^{in(\varphi-\varphi_0)}$$

we can derive:

$$D_1 \frac{\partial P_s^{(1)}}{\partial \rho}|_{\rho=a} = \sum_{n=0}^{\infty} C_n D_1 e^{-\lambda_n t} J_n(k_\rho \rho_0) J_n'(k_\rho a) k_\rho e^{in(\varphi-\varphi_0)} \quad \text{(A-1)}$$

$$M P_s^{(1)}|_{\rho=a} = \sum_{n=0}^{\infty} C_n M e^{-\lambda_n t} J_n(k_\rho \rho_0) J_n(k_\rho a) e^{in(\varphi-\varphi_0)} \quad \text{(A-2)}$$

Incorporating Eq. (A-1)-(A-2) into our initial boundary condition for the permeable membrane, Eq. (4):

$$D_1 \frac{\partial P_s^{(1)}}{\partial \rho}|_{\rho=a} + M P_s^{(1)}|_{\rho=a} = 0$$

gives us:

$$\sum_{n=0}^{\infty} C_n e^{-\lambda_n t} J_n(k_\rho \rho_0)[D_1 J_n'(k_\rho a) k_\rho + M J_n(k_\rho a)] e^{in(\varphi-\varphi_0)} = 0 \quad \text{(A-3)}$$

which is equivalent to:

$$D_1 J_n'(k_\rho a) k_\rho + M J_n(k_\rho a) = 0 \quad \text{(A-4)}$$

The parameters we defined earlier, $k_\rho = \frac{\alpha_{nm}}{a}$ and $h = \frac{aM}{D_1}$, have been integrated into Eq. (A-4). We derive our boundary condition in Eq. (15):

$$\alpha_{nm} J_n'(\alpha_{nm}) + h J_n(\alpha_{nm}) = 0$$

APPENDIX B

Here we demonstrate how we derive the normalizing constants A_{nm} in Eqs. (16)-(17). Based on the orthogonality of Bessel functions, we have:

$$\begin{aligned} \int_0^a \rho J_n(k_i\rho) J_n(k_j\rho) d\rho &= 0 (i \neq j) \\ &= N_i (i = j) \end{aligned} \quad \text{(A-5)}$$

where

$$N_i = \frac{a^2}{2}\{[J_n'(k_i a)]^2 + (1 - \frac{n^2}{a^2 k_i^2}) J_n^2(k_i a)\} \quad \text{(A-6)}$$

We define $k_i = \frac{\alpha_{nm}}{a}$ as before and can rewrite Eq. (A-6) as:

$$N_{nm} = \frac{a^2}{2}[J_n'(\alpha_{nm})]^2 + (1 - \frac{n^2}{\alpha_{nm}^2}) J_n^2(\alpha_{nm}) \quad \text{(A-7)}$$

Given our boundary condition Eq. (15): $\alpha_{nm} J_n'(\alpha_{nm}) + h J_n(\alpha_{nm}) = 0$, we can derive:

$$N_{nm} = \frac{a^2}{2}(\frac{h^2 + \alpha_{nm}^2 - n^2}{\alpha_{nm}^2}) J_n^2(\alpha_{nm}) \quad \text{(A-8)}$$

In order to derive our normalizing constant A_{nm} in Eqs. (16)-(17), we integrate Eq. (14), the propagator, on the cylindrical cross section at time $t = 0, \rho = \rho_0, \varphi = \varphi_0$ and $P_s^{(1)} = \delta(\vec{r} - \vec{r}_0)$:

$$\int\int P_s^{(1)} ds = 1 \quad \text{(A-9)}$$

Therefore, we have:

$$A_{nm}^2 \int_{\rho=0}^{\rho=a} \int_{\varphi=0}^{\varphi=2\pi} \rho J_n^2(\frac{\alpha_{nm}}{a}\rho) \cos^2(n\varphi) d\rho d\varphi = 1 \quad \text{(A-10)}$$

Given that:

$$\begin{aligned} \int_0^{2\pi} \cos^2(n\varphi) d(\varphi) &= \pi (n \neq 0) \\ &= 2\pi (n = 0) \end{aligned} \quad \text{(A-11)}$$

we can derive A_{nm}^2 based on Eq. (A-8) and Eq. (A-11),

$$\begin{aligned} A_{nm}^2 &= \frac{1}{2\pi}\frac{1}{N_n} (n = 0) \\ &= \frac{1}{\pi}\frac{1}{N_n} (n \neq 0) \end{aligned} \quad \text{(A-12)}$$

which is equivalent to the following in Eqs. (16)-(17):

$$A_{0m}^2 = \frac{1}{\pi a^2} \frac{\alpha_{0m}^2}{J_0^2(\alpha_{0m})(h^2 + \alpha_{0m}^2)} \quad \text{(A-13)}$$

$$A_{nm}^2 = \frac{2}{\pi a^2} \frac{\alpha_{nm}^2}{J_n^2(\alpha_{nm})(h^2 + \alpha_{nm}^2 - n^2)}, n \neq 0 \quad \text{(A-14)}$$

References

[1] D. Alexander. A general framework for experiment design in diffusion MRI and its application in measuring direct tissue-microstructure features. *Magnetic Resonance in Medicine*, 60(2):439–48, 2008.

[2] Y. Assaf, T. Blumenfeld, G. Levin, Y. Yovel, and P. Basser. AxCaliber-A method to measure the axon diameter distribution and density in neuronal tissues. In *Proceedings of the 14th ISMRM Scientific Meeting*, volume 40, 2006.

[3] L. Avram, Y. Assaf, and Y. Cohen. The effect of rotational angle and experimental parameters on the diffraction patterns and micro-structural information obtained from q-space diffusion NMR: implication for diffusion in white matter fibers. *Journal of Magnetic Resonance*, 169(1):30–38, 2004.

[4] K. Brownstein and C. Tarr. Importance of classical diffusion in NMR studies of water in biological cells. *Physical Review A*, 19(6):2446–2453, 1979.

[5] P. Callaghan. Pulsed-gradient spin-echo NMR for planar, cylindrical, and spherical pores under conditions of wall relaxation. *Journal of Magnetic Resonance, Series A*, 113(1):53–59, 1995.

[6] M. Hall and D. Alexander. Finite pulse width improve fibre orientation estimates in diffusion tensor MRI. *Proc. ISMRM*, page 1076, 2006.

[7] C. Meier, W. Dreher, and D. Leibfritz. Diffusion in compartmental systems. II. Diffusion-weighted measurements of rat brain tissue in vivo and postmortem at very large b-values. *Magnetic Resonance in Medicine*, 50(3):510–514, 2003.

[8] C. Meier, W. Dreher, and D. Leibfritz. Diffusion in compartmental systems. I. A comparison of an analytical model with simulations. *IEEE Trans Med Imag*, 26:1437–1447, 2007.

[9] M. Nilsson, J. Lätt, E. Nordh, R. Wirestam, F. Stĺhlberg, and S. Brockstedt. On the effects of a varied diffusion time in vivo: is the diffusion in white matter restricted? *Magnetic Resonance Imaging*, 2008.

[10] J. Pfeuffer, U. Floègel, W. Dreher, and D. Leibfritz. Restricted diffusion and exchange of intracellular water: theoretical modelling and diffusion time dependence of H NMR measurements on perfused glial cells. *NMR in Biomedicine*, 11:19–31, 1998.

[11] W. Price, A. Barzykin, K. Hayamizu, and M. Tachiya. A model for diffusive transport through a spherical interface probed by pulsed-field gradient NMR. *Biophysical Journal*, 74(5):2259–2271, 1998.

[12] J. Ritchie. On the relation between fibre diameter and conduction velocity in myelinated nerve fibres. *Proceedings of the Royal Society of London. Series B, Biological Sciences (1934-1990)*, 217(1206):29–35, 1982.

[13] J. Sehy, A. Banks, J. Ackerman, and J. Neil. Importance of intracellular water apparent diffusion to the measurement of membrane permeability. *Biophysical Journal*, 83(5):2856–2863, 2002.

[14] S. Waxman. Determinants of conduction velocity in myelinated nerve fibers. *Muscle Nerve*, 3(2):141–50, 1980.

[15] J. Weng, J. Chen, L. Kuo, V. Wedeen, and W. Tseng. Maturation-dependent microstructure length scale in the corpus callosum of fixed rat brains by magnetic resonance diffusion–diffraction. *Magnetic Resonance Imaging*, 25(1):78–86, 2007.